Spiral magnetic states in the large-U Hubbard model: a slave boson approach

1992 J. Phys.: Condens. Matter 4 3625

(http://iopscience.iop.org/0953-8984/4/13/022)

J. Phys.: Condens. Matter 4 (1992) 3625–3638. Printed in the UK

Spiral magnetic states in the large-U Hubbard model: a slave boson approach

Raymond Frésard and Peter Wölfle

Institut für Theorie der Kondensierten Materie, Universität Karlsruhe, Physikhochhaus, 7500 Karlsruhe, Federal Republic of Germany

Received 1 November 1991

Abstract. We determine the ground state phase diagram of the Hubbard model on the square lattice allowing for homogeneous spiral, antiferromagnetic, ferromagnetic and paramagnetic phases. This is obtained from a saddle-point approximation of a spin-rotation-invariant form of the slave boson representation introduced by Kotliar and Ruckenstein. We obtain very good agreement in energy with exact diagonalization calculations and, concerning the magnetic structure, qualitative agreement with experimental data.

1. Introduction

Recently there has been a revival of interest in the magnetic properties of the large repulsive U Hubbard model, following the suggestion by Anderson [1] that the model should capture the essential physics of the cuprate superconductors. Earlier attempts to determine the magnetic phase diagram (for an overview see the book by Mattis [2]) indicated the existence of antiferromagnetic order in the region of the phase diagram around half-filling and ferromagnetic order for intermediate density and large interaction strength. Obviously, antiferromagnetic and ferromagnetic order compete at finite doping of the half-filled band. It is by now well established that there is antiferromagnetic long range order, with a charge excitation gap, in the ground state of the Hubbard model with nearest-neighbour hopping on a two-dimensional square lattice at half-filling [3]. Several different approaches suggest that the antiferromagnetic order is destroyed upon doping. However, it is difficult to calculate the effect of mobile holes on a spin background in a controlled way. In the restricted Hartree–Fock approximation (HFA) antiferromagnetic, ferromagnetic and ferrimagnetic phase regions have been found [4], with the AF region extending out to high doping levels. At larger interaction strength U, where the Hartree–Fock approximation is expected to be less reliable, the Gutzwiller variational approximation (GA) has been applied [5], with results qualitatively similar to Hartree–Fock. The main differences in the phase diagram appear at low density, where HFA yields a ferromagnetic phase for sufficiently large U, whereas GA stabilizes the paramagnetic state for all U. All these results show a region of phase separation (i.e. a mixture of two phases with different magnetic order and density) at larger doping levels. However, whether phase separation is a true property of the Hubbard model remains to be seen. Exact (numerical) quantum Monte Carlo calculations for systems of dimensions up to 8×8 have so far not shown

0953-8984/92/133625+14$04.50

any sign of phase separation. Should it turn out that phase separation occurs in the ground state of the Hubbard model for some region of the phase diagram, this would signal the inadequacy of the approximations leading to the Hubbard model in the first place. A finite range interaction or possibly the infinite range Coulomb interaction term would have to be added to the Hubbard model in that case. Whether phase separation still occurs within such a more realistic model is an open question.

We think it worthwhile to explore the possibility of stable translation-invariant ground states of the Hubbard model. The tendency towards phase separation is clearly related to the competition of the antiferromagnetic exchange interaction derived from the Hubbard model and the kinetic energy of holes in the half-filled band, favouring ferromagnetic or paramagnetic spin background over an antiferromagnetic one. The two tendencies may be at least partially satisfied by magnetic structures representing a compromise, such as incommensurate spiral magnetic states (SM), canted spin states (CS), ferrimagnetic states (FIM), linearly polarized spin density waves (LSDW) and others. Among these, incommensurate spiral magnetic order is of particular interest, since incommensurate medium-ranged magnetic order has been detected in $La_{2-x}Sr_xCuO_4$ by neutron scattering experiments [6, 7]. Theoretical support for spiral order comes from the analysis of Shraiman and Siggia [8], who demonstrated the existence of interaction terms favouring spiral order in an effective classical field theory of doped antiferromagnets. The effect of quantum fluctuations in spiral phases has been considered in [9], and a double spiral structure has been identified as the lowest energy state there. Already in the Hartree–Fock approximation a spiral magnetic solution is found to be lower in energy that the AF state for any finite doping [10–12]. Recently more complex solutions of the Hartree–Fock theory have been studied, such as domain-wall structures of various kinds [13–16]. Since the Hartree–Fock theory ceases to be controlled at larger values of U, and since the discussion of spiral order given in [8] is valid at most in the limit of low hole density, more generally applicable theories are greatly needed. In this paper we present results on incommensurate spiral magnetic states obtained within a slave boson mean-field theory comparable to the Gutzwiller approximation.

2. Spin-rotation invariant slave boson representation

We consider the Hubbard model for electrons on the square lattice:

$$H = \sum_{\langle i,j\rangle,\sigma} t_{i,j}\, c^{+}_{i,\sigma} c_{j,\sigma} + U \sum_{i} n_{i,\uparrow} n_{i,\downarrow} \tag{1}$$

with nearest-neighbour hopping matrix elements $t_{i,j} = -t$. Using a spin-rotation-invariant form [17] of the slave boson (SB) representation introduced by Kotliar and Ruckenstein [18], the electron operator $c_{i,\sigma}$ is expressed in terms of pseudofermion operator $f_{i,\sigma}$ and slave boson operators $e_i, d_i, p_{i,\mu}, \mu = 0,1,2,3$ for the empty, doubly and singly occupied sites, as

$$c_{i,\sigma} = \sum_{\sigma'} f_{i,\sigma'} z_{i,\sigma',\sigma} \tag{2}$$

where

$$\underline{z} = [(1 - d^{+}d)\underline{\tau}_0 - \underline{p}^{+}\underline{p}]^{-1/2}[e^{+}\underline{p} + \underline{\tilde{p}}^{+}d][(1 - e^{+}e)\underline{\tau}_0 - \underline{\tilde{p}}^{+}\underline{\tilde{p}}]^{-1/2} \tag{3}$$

and

$$\underline{p}_i = \frac{1}{\sqrt{2}} \sum_\mu p_{i\mu} \underline{\tau}_\mu . \tag{4}$$

Here the τ_μ are the Pauli matrices, including the unit matrix ($\mu = 0$), $\bar{p}$ is the time reversed operator p, and the underbar denotes 2×2 spin matrices. The projection onto the physical subspace is implemented by a set of constraints. For details of the representation we refer to a separate publication [19].

The partition function of the Hubbard model may be expressed as a path integral over coherent states of the slave bosons

$$Z = \int D[e, p_0, p]\, D[d, d^+]\, D[\alpha, \beta_0, \beta] \mathrm{e}^{-(S^B + S^F)} \tag{5}$$

where the bosonic and fermionic parts of the action are given by

$$S^B = \int_0^{1/T} \mathrm{d}\tau \sum_i \{ d_i^+ [\partial_\tau + \alpha_i - 2\beta_{i0} + U] d_i + \alpha_i (e_i^2 - 1) + (\alpha_i - \beta_{i0}) \sum_\mu p_{i\mu}^2 - 2\beta_i \cdot p_i p_{i0} + h \cdot p_i p_{i0} \} \tag{6}$$

and

$$S^F = \mathrm{Tr} \ln \left\{ [(\partial_\tau - \mu + \beta_{i0}) \delta_{\sigma,\sigma'} + \beta_i \cdot \tau_{\sigma,\sigma'}] \delta_{i,j} + t_{i,j} \sum_{\sigma_1} z^+_{i,\sigma_1,\sigma} z_{j,\sigma',\sigma_1} \right\} \tag{7}$$

In the expression for S^F Tr denotes a trace over time, space and spin. The five slave boson fields e, p_0, p are real valued and are integrated like radial parts of complex fields, i.e. $\int_0^\infty \mathrm{d}e^2 \ldots$, and so forth, whereas α, β_0, β are integrated along the imaginary axis from $-\mathrm{i}\infty$ to $\mathrm{i}\infty$. The boson d representing doubly occupied sites is the only complex field as discussed in [19, 20]. In S^B, h denotes an applied magnetic field and in S^F μ is the chemical potential.

Saddle point approximations to (5) are obtained by replacing the Bose fields by their time averaged values. These values are determined by minimizing the corresponding mean-field energy $F_{MF} = -T \ln Z_{MF}$. A spiral magnetic state is characterized by a magnetization vector varying in space as

$$M_i = M \hat{n}_i \tag{8}$$

where the unit vector $\hat{n}_i$ forms a spiral structure, e.g.

$$\hat{n}_i = (\cos \phi_i, \sin \phi_i, 0) \tag{9}$$

with the site dependent rotation angle

$$\phi_i = Q \cdot R_i \qquad R_i = a(n_1, n_2). \tag{10}$$

The simplifying feature of this type of structure is that the length of the magnetization vector is uniform in space, only the direction varies. The spiral state is completely

defined by the wavevector Q. Limiting cases are the antiferromagnet with $Q = \pi/a(1,1)$ and the ferromagnet where $Q = 0$.

The spatial variation of the mean-field values of the Bose fields is dictated by the form of M_i. All quantities transforming as vectors in spin space must show the same variation. Hence

$$p_i = p\hat{n}_i \qquad \beta_i = \beta\hat{n}_i \tag{11}$$

whereas the scalar bosons e, d, p_0 and α, β_0 are taken to be uniform in space.

In terms of the eigenvalues $\lambda_\pm$ and eigenvectors $\chi_{i\pm}$ of the matrix $\underline{p}_i$ at each lattice site,

$$\lambda_\nu = p_0 + \nu p \tag{12}$$

$$\chi_i^\nu = \frac{1}{\sqrt{2}} \begin{pmatrix} \nu e^{-i\phi_i} \\ 1 \end{pmatrix} \qquad \nu = \pm 1 \tag{13}$$

the matrix $\underline{z}_i$ may be expressed in terms of its eigenvalues as

$$\underline{z}_i = \tfrac{1}{2} \sum_{\nu=\pm 1} \chi_i^\nu \chi_i^{\nu+} L_{i,\nu}(e\lambda_\nu + d\lambda_{-\nu}) R_{i,-\nu} \tag{14}$$

where

$$L_{i,\nu} = [1 - d^2 - \tfrac{1}{2}(p_0 + \nu p)^2]^{-1/2} \tag{15}$$

$$R_{i,\nu} = [1 - e^2 - \tfrac{1}{2}(p_0 + \nu p)^2]^{-1/2}. \tag{16}$$

Explicitly, one obtains

$$\underline{z}_i = \begin{pmatrix} z_+ & z_- e^{-i\phi_i} \\ z_- e^{i\phi_i} & z_+ \end{pmatrix} \tag{17}$$

with

$$z_\pm = B_+ L_+ R_- \pm B_- L_- R_+ \tag{18}$$

and

$$B_\pm = \frac{1}{2\sqrt{2}}[p_0(e + d) \pm p(e - d)]. \tag{19}$$

Next the trace in the expression (7) for S^F has to be evaluated. The matrix quantity under the trace may be diagonalized by a Fourier transformation in space and time. Consider the matrix elements of the hopping term in the momentum representation:

$$\underline{T}_{k,k',\sigma,\sigma'} \equiv \sum_{i,j,\sigma_1} e^{ik\cdot R_i} t_{i,j} z^+_{i,\sigma_1,\sigma} z_{j,\sigma',\sigma_1} e^{ik'\cdot R_j} \tag{20}$$

substituting the expression (17) for $\underline{z}$ and performing the summation on R_i, R_j one finds

$$\underline{T}_{k,k'} = \begin{pmatrix} (z_+^2 t_k + z_-^2 t_{k+Q})\delta(k-k') & z_+ z_- (t_k + t_{k+Q})\delta(k-k'+Q) \\ z_+ z_- (t_k + t_{k-Q})\delta(k-k'-Q) & (z_+^2 t_k + z_-^2 t_{k-Q})\delta(k-k') \end{pmatrix} \tag{21}$$

with

$$t_k = \sum_{i,j} t_{i,j} e^{ik\cdot(R_i - R_j)} = -2t(\cos k_x a + \cos k_y a) \qquad \delta(k-k') = \sum_j e^{i(k-k')\cdot R_j}. \tag{22}$$

Including the chemical potential terms, the fermionic part of the action, (7) may be expressed as

$$S^F = T \sum_{\omega_n} \mathrm{Tr}_k \ln[i\omega_n \delta(k-k') - \underline{E}_{k,k'}] \tag{23}$$

where the quasiparticle energy matrix is defined by

$$\underline{E}_{k,k'} = \begin{pmatrix} e_1(k)\delta(k-k') & e_2(-k)\delta(k-k'+Q) \\ e_2(k)\delta(k-k'-Q) & e_1(-k)\delta(k-k') \end{pmatrix} \tag{24}$$

with elements

$$e_1(k) = (z_+^2 t_k + z_-^2 t_{k+Q}) + \beta_0 - \mu_0 \qquad e_2(k) = z_+ z_- (t_k + t_{k-Q}) + \beta. \tag{25}$$

The energy matrix can be diagonalized easily since only pairs of k values are coupled. Writing out the eigenvalue equation

$$\sum_{k'} [\underline{E}_{k,k'} - \underline{1} E \delta(k-k')] \psi_{k'} = 0 \tag{26}$$

with

$$\psi_k = \begin{pmatrix} \psi_{1,k} \\ \psi_{2,k+Q} \end{pmatrix} \tag{27}$$

then for each k a closed system of two equations is obtained:

$$(e_1(k) - E)\psi_{1,k} + e_2(-k)\psi_{2,k+Q} = 0 \tag{28}$$

$$e_2(k)\psi_{1,k} + (e_1(-k) - E)\psi_{2,k+Q} = 0. \tag{29}$$

The energy eigenvalues follow from the zeros of the 2×2 determinant of coefficients as

$$E_{k,\nu} = \tfrac{1}{2}(z_+^2 + z_-^2)(t_k + t_{k+Q}) + \beta_0 - \mu \pm \tfrac{1}{2}\{(z_+^2 - z_-^2)^2 (t_k - t_{k+Q})^2 + 4[z_+ z_- (t_k + t_{k+Q}) + \beta]^2\}^{1/2} \qquad \nu = \pm 1. \tag{30}$$

The mean-field free energy follows as

$$F = -T\sum_{k,\nu} \ln[1 + \exp(E_{k,\nu}/T)] + Ud^2 + \alpha(e^2 + d^2 + p_0^2 + p^2 - 1)$$
$$- \beta_0(2d^2 + p_0^2 + p^2) - 2\beta p p_0 \tag{31}$$

with the saddle point values of the Bose fields being determined by the Euler–Lagrange equations

$$\partial F/\partial e = 2\alpha e + \sum_{\nu}(\partial z_\nu^2/\partial e)U_\nu = 0$$

$$\partial F/\partial d = 2(U + \alpha - 2\beta_0)d + \sum_{\nu}(\partial z_\nu^2/\partial d)U_\nu = 0$$

$$\partial F/\partial p_0 = 2(\alpha - \beta_0)p_0 - 2\beta p + \sum_{\nu}(\partial z_\nu^2/\partial p_0)U_\nu = 0$$

$$\partial F/\partial p = 2(\alpha - \beta_0)p - 2\beta p_0 + \sum_{\nu}(\partial z_\nu^2/\partial p)U_\nu = 0$$

$$\partial F/\partial \alpha = e^2 + d^2 + p_0^2 + p^2 - 1 = 0$$
$$\partial F/\partial \beta_0 = -(2d^2 + p_0^2 + p^2) + n = 0$$
$$\partial F/\partial \beta = -2pp_0 + m = 0 \tag{32}$$

and

$$\partial F/\partial Q = \sum_{k,\nu} f(E_{k,\nu})\nabla_Q E_{k,\nu} = 0. \tag{33}$$

Here we have defined ($f(E)$ is the Fermi function)

$$U_\nu = \sum_{k,\nu'} f(E_{k,\nu'})\frac{\partial E_{k,\nu'}}{\partial z_\nu^2} \tag{34}$$

the density

$$n = \sum_{k,\nu} f(E_{k,\nu}) \tag{35}$$

and the amplitude of the spiral spin density wave

$$m = \sum_{k,\nu} f(E_{k,\nu})\frac{\partial E_{k,\nu}}{\partial \beta}. \tag{36}$$

3. Numerical solution of saddle point equations and results

To solve the set of equations (32) and (33) we proceed as follows: for fixed spiral wavevector Q we eliminate the variables $e, p, d, \alpha, \beta_0, \beta$ at the price of introducing U_ν and m as unknown variables. The remaining equation for p_0 is

$$U(4p_0^4 - m^2) = \sum_\nu z_\nu U_\nu \left[(m^2 - 4p_0^4) \left(\frac{1}{e}\frac{\partial z_\nu}{\partial e} + \frac{1}{d}\frac{\partial z_\nu}{\partial d} \right) - 4mp_0 \frac{\partial z_\nu}{\partial p} + 8p_0^3 \frac{\partial z_\nu}{\partial p_0} \right]. \tag{37}$$

The variables e, p, d are obtained from the constraints, while α, β_0, β are given by

$$\alpha = \frac{-1}{2e} \sum_\nu U_\nu \frac{\partial z_\nu^2}{\partial e} \qquad \beta_0 = \frac{U}{2} + \frac{1}{4} \sum_\nu U_\nu \left(\frac{1}{d}\frac{\partial z_\nu^2}{\partial d} - \frac{1}{e}\frac{\partial z_\nu^2}{\partial e} \right)$$

$$\beta = \frac{-mU}{4p_0^2} + \sum_\nu U_\nu \left[\frac{1}{2p_0}\frac{\partial z_\nu^2}{\partial p} - \frac{m}{8p_0^2} \left(\frac{1}{e}\frac{\partial z_\nu^2}{\partial e} + \frac{1}{d}\frac{\partial z_\nu^2}{\partial d} \right) \right]. \tag{38}$$

Solving (37) at the point where U_ν and m are stationary yields the saddle point. While this is easily achieved by the usual iteration technique for moderate interaction strength U, up to $10t$, one really has to solve the three stationary equations, in which the non-linearity becomes essential, for larger value of U. Working at a fixed value of m, we are left with solving the two equations $g_\nu = 0$ where

$$g_\nu \equiv U_\nu^{\mathrm{it}}(\{U_\mu\}, m, p_0) - U_\nu \qquad \nu = \pm 1. \tag{39}$$

Starting from $(\{U_\nu\}, m)$, firstly determining p_0 with (37), we then use (38) to obtain e, p, α, β_0 and β. Using the definitions (34) and (36) allows us to determine U_ν^{it}. The two equations $g_\nu = 0$ are then solved by the 'double bisection' method. We can then determine m and finally look for the spiral wavevector which is minimizing F. We worked on a 98×98 lattice, and, since this method is particularly time consuming but not limited in principle, we restricted our calculations to $U \leqslant 20t$.

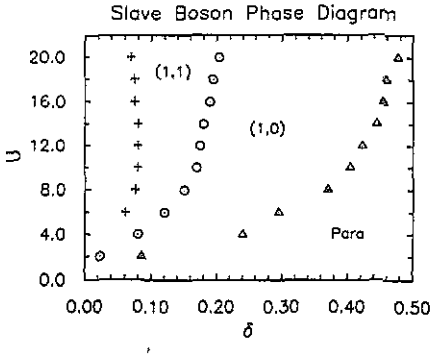

Figure 1. Ground state phase diagram of the Hubbard model. The AF state takes place at half-filling only. The circles denote the phase boundary between the $(1,1)$ and $(1,0)$ spiral phases, and the triangles the boundary between the $(1,0)$ spiral and the paramagnetic phase. The crosses represent the line of zero compressibility, separating single phase and phase separated states.

In figure 1 we show the (U, δ) phase diagram that we obtained by solving the saddle point equations (32) and (33) for $0 \leqslant U/t \leqslant 20$, thus completing a previous study [21]. It turns out that the spiral wavevectors which are minimizing the energy belong to two different families: either $Q = (\pi - \delta Q_x)(1,1)$ (hereafter denoted by $(1,1)$), or $Q = \pi(1,1) - \delta Q_x(1,0)$ (denoted by $(1,0)$). At half-filling we obtain the AF state as ground state. Upon doping it becomes immediately unstable towards a $(1,1)$ spiral phase. For small doping this phase is characterized by a negative compressibility and is therefore unstable with respect to phase separation. Beyond a critical doping value indicated in figure 1 the compressibility of the $(1,1)$ spiral phase turns positive and consequently this state is thermodynamically stable. This is in contrast to the HF solution, for which the regime of instability is much more extended [12, 22]. When the doping is increased, the system undergoes a first-order phase transition towards a $(1,0)$ spiral phase. The latter phase is characterized by a large magnetization around the transition (~ 0.5) and a very small (and even vanishing) magnetic gap (as defined by the energy separation of the two bands $E_{k\pm}$). When the doping is again increased there is a second order phase transition to the paramagnetic state. It has to be noted that the ferromagnetic (F) state is absent within this parameter range. Extrapolating our data for larger U at a given density indicates that the F state shows up for $U \geqslant 40t$ for $\delta \sim 16\%$, and at higher values of U for other densities.

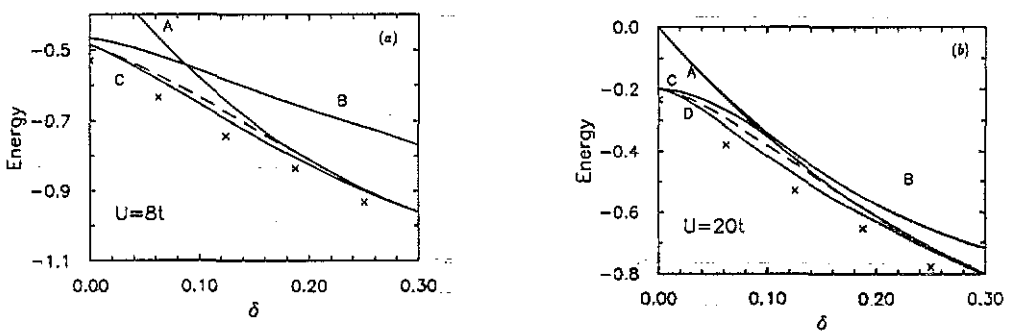

Figure 2. Comparison of ground state energies against hole concentration obtained from the slave boson approximation (SB) and Hartree–Fock approximation (HF) with exact diagonalization data. (*a*) SB results for the paramagnetic state (A), for the antiferromagnetic state (broken curve) and for the spiral state (C); HF results for the spiral state (B); and exact diagonalization data (crosses) for $U = 8t$. (*b*) Shown are SB results for the paramagnetic state (A), for the ferromagnetic state (B), for the antiferromagnetic state (dashed curve) and for the spiral state (D); HF results for the spiral state (C); exact diagonalization data (crosses) for $U = 20t$.

In figure 2(*a*) we show the ground state energy for $U = 8t$ as a function of the density as obtained from our slave boson calculation for the best spiral wavevector. We compare it with Hartree–Fock results [12] and exact diagonalization on a 4×4 lattice [23]. As we already pointed out for a smaller interaction strength, $U = 4t$ [24], the agreement between SB and HF is very severely affected upon doping. Contrary to this the agreement between SB and exact diagonalization is improved upon doping to be as good as showing a difference less than 4% for $\delta > 15\%$, i.e. three holes and more in the 4×4 lattice. That the agreement is not so good around half-filling is not surprising since our saddle point approach does not account for the quantum fluctuations which are lowering the energy from $-J$ down to $\sim -1.15J$ in the large

U limit. Nevertheless our results are within 8% of the exact diagonalization results at half-filling.

Moreover, taking the spiral state into consideration allows a lowering of the energy from the AF state by as much as 2.5% for a doping of 8%. One can also notice that the spiral phase is stable over a much wider density domain than the antiferromagnetic phase.

We carried out the same comparison for $U = 20t$, as shown on figure 2(b). The increase in the interaction strength leads to a bigger difference between slave boson and exact diagonalization results. The difference goes from $\sim$ 15% at half-filling down to 7% when the doping is larger than 15%. We also included the ferromagnetic state in our comparison but figure 2(b) clearly shows that for $U = 20t$ the slave boson mean-field approach, even in the paramagnetic state, gives lower energies.

In figure 3 we display the ground state energies as functions of the density for $U/t = 4$, 8, 12 and 18. The tendency towards instability (i.e. negative compressibility) which is essentially absent for $U/t = 6$ and smaller, is first enhanced by increasing the interaction strength, and then, for $U \geqslant 14t$, restricted to smaller and smaller doping regions. The tendency towards phase separation is enhanced by increasing U. Nevertheless it has to be noted that the doping domain where the energy can be lowered by the Maxwell construction is considerably smaller than the one obtained in the framework of mean-field theory [12, 22].

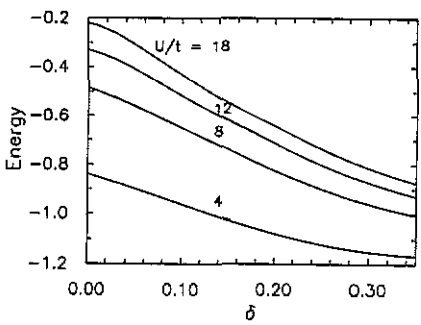

Figure 3. Slave boson ground state energies against hole concentration for $U/t = 4$, 8, 12 and 18.

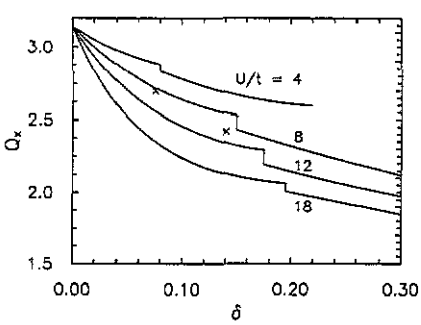

Figure 4. Comparison of the x component of the spiral wavevector against hole concentration obtained from the slave boson (SB) approach with the experimental data. Shown are SB results for $U/t = 4$, 8, 12 and 18; experimental data (crosses).

Figure 4 shows the x component of the spiral wavevector as a function of the doping for $U/t = 4$, 8, 12 and 18 (the jumps indicate the transition from $(1,1)$ to $(1,0)$). The departure of Q_x from π is given approximately by $\delta Q_x = \delta U/t$ for small doping. For higher doping this linear behaviour in δ is no longer true and Q_x always saturates in the $(1,1)$ regime, then jumps to the $(1,0)$ regime and saturates again. Therefore the F state, as well as the $Q = (0,\pi)$ state, which occur in the Hartree–Fock phase diagram in the parameter range for U and δ considered here, do not appear in our slave boson calculation.

In figure 4 we also included the experimental data of Cheong *et al* [7] who measured the neutron scattering cross section of $La_{2-x}Sr_xCuO_4$ and found incommensurate medium-range magnetic order with a wavevector (Q_x,π) for $x \geqslant 7\%$. Assuming that the hole doping is equal to the concentration of Sr, we see that the two experimental points are in qualitative agreement with the slave boson theory. Indeed in this part of the phase diagram, for $U/t \cong 4$ and $\delta \geqslant 7\%$, our mean field approach predicts $(1,0)$ ordering with values of Q_x in qualitative agreement with the experiment.

For small doping, i.e. in the $(1,1)$ regime, the Fermi surface consists of one hole pocket located arond $(\pi/2,\pi/2)$, the size of which increases upon doping. At the $(1,1)$ to $(1,0)$ transition it changes completely to become an asymmetric stripe which runs around one half of the magnetic Brillouin zone; this stripe is infinitely long in one direction and not in the other. Nevertheless one has to keep in mind that the spiral states associated with all the $Q = (\pm Q_x, \pm Q_y)$ are degenerate in energy. This restores the expected symmetry of the Fermi surface. Other evidence for incommensurate magnetic order are provided by quantum Monte Carlo calculations on finite lattices [25]. However, due to the small size of the lattices that have been studied and the relatively large temperature, it is quite unlikely that incommensurate long-range order can be detected from the simulations, in contrast to short-range order. Indeed it is found, for $U \sim 4t$, that the position of the maximum of the magnetic structure factor moves away from (π,π) to the side of the Brillouin zone upon doping, which is consistent with our slave boson results. According to exact diagonalization results the same behaviour occurs in the t–J model, even though it is not quite clear whether the maximum of the magnetic structure factor moves away from (π,π) for arbitrary small doping, or only when it exceeds a certain threshold [26].

Figure 5 displays the magnetization as a function of the doping for $U/t = 4$, 8, 12 and 18. The linear behaviour of m in the $(1,0)$ domain, which was already observed for $U/t = 4$ [24], is also present for the other values of U. One can also remark that the jump in m at the transition increases as a function of the interaction strength. The ferromagnetic behaviour, i.e. $m = n$, is not seen at all in this calculation. Therefore the tendency of MF calculations to overestimate the amplitude of the spin–spin correlation functions is noticeably reduced with respect to HF.

Figure 6 shows the density of doubly occupied sites as a function of the doping for $U/t = 4$, 8, 12 and 18. The transition from the $(1,1)$ to the $(1,0)$ domain is accompanied by a discontinuous increase in d^2. The size of the jump is lowered by increasing U.

Figure 7 shows the Lagrange multiplier β as a function of the doping for $U/t = 4$, 8, 12 and 18. In the AF state, β plays the role of the magnetic gap. At half-filling, β grows like $U/2t$ for large U. However, it is quite remarkable that β is very

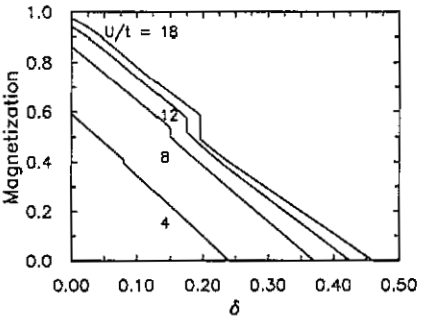

Figure 5. Magnetization against hole concentration for $U/t = 4$, 8, 12 and 18.

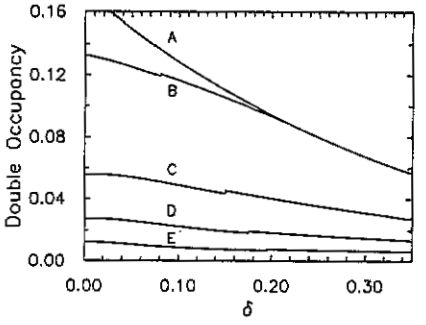

Figure 6. Density of doubly occupied sites against hole concentration. Shown are the results in the paramagnetic phase for $U/t = 4$ (A); in the spiral phase for $U/t = 4$ (B), 8 (C), 12 (D), 18 (E).

strongly suppressed upon doping, rapidly becoming of order t, before vanishing at the paramagnetic transition.

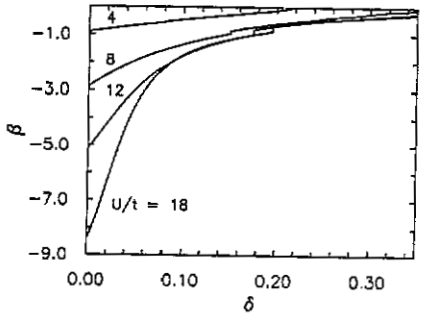

Figure 7. Lagrange multiplier β (see text) against hole concentration for $U/t = 4$, 8, 12 and 18.

Figure 8 shows the magnetic gap, defined as $\Delta = \min(E_{k+} - E_{k-})$ for positive $(E_{k+} - E_{k-})$ and zero elsewhere, as a function of the density for $U/t = 4$, 8, 12 and 18. Whereas Δ is well approximated by U at half-filling, particularly for the largest values of U, it is very strongly reduced upon doping, vanishing already in the $(1,1)$ domain. It then suddenly reappears at the $(1,1)$ to $(1,0)$ transition. This has to be

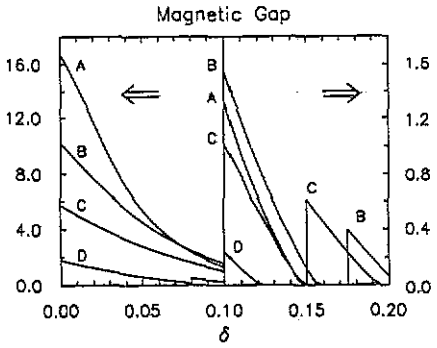

Figure 8. Magnetic gap Δ against hole concentration for $U/t = 18$ (A), 12 (B), 8 (C), 4 (D). The jumps correspond to the transition from $(1,1)$ to $(1,0)$ spiral states.

contrasted with the Hartree–Fock result where, for large U, one finds $\Delta_{\mathrm{HF}} \sim Un$, even for finite doping. This has a particularly strong influence on the band width. The latter is shown in figure 9 as a function of the density for $U/t = 4$, 8, 12 and 18. For the sake of clarity we consider the lower magnetic subband only, even though the two bands overlap when the magnetic gap vanishes (see figure 8). We see at half-filling that increasing U reduces the band width, which indeed scales with $16t^2/U$ $(= 4J$ where J is the exchange constant). Upon doping, the band width increases strongly up to the order of several t. In the t–J model, exact diagonalization calculations for the system doped with one hole have shown the quasi-particle band width to be $2J$, with a dispersion relation well reproduced (up to a constant term) by $(J/8)t_{\mathrm{k}}^2 - J$ [27, 28]. A similar dispersion relation for the quasi-particle is also obtained in our approach for large U and small doping. However, on doping, both methods show a drastic increase of the band width and a qualitative change of the dispersion relation towards the bare hopping renormalized by an effective mass [29].

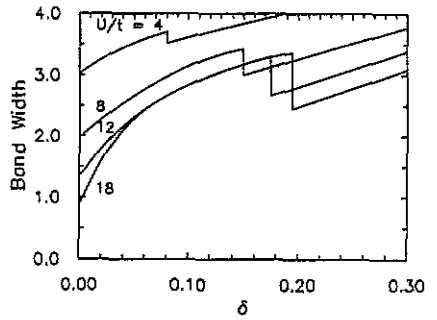

Figure 9. Band width in the spiral state against hole concentration for $U/t = 4$, 8, 12 and 18.

The strong reduction of the magnetic gap on doping also affects the density of states. The spectral weight carried by the upper magnetic subband will gradually be transferred to the lower subband on doping. For instance, for $U = 12t$, we are left with one single band for $\delta \geqslant 15\%$. The transfer of spectral weight from the upper to the lower Hubbard band upon doping has been seen using the exact diagonalization method [23]. However, even though the upper Hubbard band is affected by doping, it always carries a finite spectral weight, contrary to our mean-field approach. One

expects to retrieve the full contribution of the upper Hubbard band from a proper calculation of the Gaussian fluctuations [19].

4. Conclusion

We applied the slave boson mean-field approach, first introduced by Kotliar and Ruckenstein [18] and made spin-rotation invariant by Li *et al* [17], to spiral magnetic states in the Hubbard model. The phase diagram is found to consist of four regions: at half-filling the ground state is antiferromagnetic. For arbitrary small doping we obtain a $(1,1)$ spiral state up to a critical doping at which the system undergoes a first-order phase transition to a $(1,0)$ spiral phase. Increasing the doping further drives the system through a second-order phase transition into the paramagnetic state. In the range of interaction strengths we considered ($U \leqslant 20t$) we did not obtain ferromagnetism. We compared our ground state energies with quantum Monte Carlo simulations [24] and with exact diagonalization results and obtained very good agreement even though the deviations were found to increase for larger interaction strengths. Part of this agreement comes from allowing for spiral states, as they lead to a substantial lowering of the ground state energy as compared to the antiferromagnetic state. We have also shown that the slave boson mean-field theory yields a drastic improvement of the Hartree–Fock weak-coupling results, particularly away from half-filling. The comparison between the spiral wavevectors that we obtained and the experimental data from neutron scattering experiments on $La_{2-x}Sr_xCuO_4$ [7], which exhibit incommensurate medium range magnetic order, shows qualitative agreement. Moreover it turns out that the magnetic gap is very strongly affected by doping, particularly for large U, and is even seen to vanish for rather small doping ($\sim 10\%$). As a consequence one obtains a transfer of spectral weight from the upper to the lower band upon doping.

Acknowledgments

One of us (RF) thanks the Fonds National Suisse pour la Recherche Scientifique for financial support. We thank Dr X Zotos and Mr M Dzierzawa for many interesting discussions and Mr B Glaser for help with the computer work.

References

[1] Anderson P W 1987 *Science* **235** 1196

[2] Mattis D C 1981 *The Theory of Magnetism I (Springer Series in Solid State Sciences 17)* ed P Fulde (Berlin: Springer)

[3] Liang S, Douçot B and Anderson P W 1988 *Phys. Rev. Lett.* **61** 365
Trivedi N and Ceperley D 1989 *Phys. Rev.* B **40** 2737

[4] Penn D R 1966 *Phys. Rev.* **142** 350
Cyrot M J 1972 *J. Physique* **33** 125

[5] Metzner W and Vollhardt D 1989 *Phys. Rev. Lett.* **62** 324
Metzner W 1989 *Z. Phys.* B **77** 253

[6] Shirane G, Birgeneau R J, Endoh Y, Gehring P, Kastner M A, Kitazawa K, Kojima H, Tanaka I, Thurston T R and Yamada K 1989 *Phys. Rev. Lett.* **63** 330
Birgeneau R J, Endoh Y, Kakurai K, Hidaka Y, Murakami T, Kastner M A, Thurston T R, Shirane G and Yamada K 1989 *Phys. Rev.* B **39** 2868

[7] Cheong S W, Aeppli G, Mason T E, Mook H, Hayden S M, Canfield P C, Fisk Z, Clausen K N and Martinez J L 1991 *Phys. Rev. Lett.* **67** 1791
[8] Shraiman B and Siggia E 1990 *Phys. Rev. Lett.* **62** 1564
[9] Kane C L, Lee P A, Ng T K, Chakravarty B and Read N 1990 *Phys. Rev.* B **41** 2653
[10] Yoshioka D 1989 *J. Phys. Soc. Japan* **58** 1516
[11] Jayaprakash C, Krishmanurthy H R and Sarker S 1989 *Phys. Rev.* B **40** 2610
[12] Dzierzawa M Z 1992 *Z. Phys.* B **86** 49
[13] Schulz H 1990 *Phys. Rev. Lett.* **64** 1445
[14] Poilblanc D and Rice T M 1989 *Phys. Rev.* B **39** 9749
[15] Bishop A R, Guinea F, Lomdahl P S, Louis E and Vergés J A 1991 *Europhys. Lett.* **14** 157
[16] Machida K 1989 *Physica* C **158** 192
Kato M, Machida K, Nakanishi H and Fujita M 1990 *J. Phys. Soc. Japan* **59** 1047
[17] Li T, Wölfle P and Hirschfeld P 1990 *Phys. Rev.* B **40** 6817
[18] Kotliar G and Ruckenstein A 1986 *Phys. Rev. Lett.* **57** 1362
[19] Frésard R and Wölfle P 1992 *Int. J. Mod. Phys.* B at press
[20] Jolicoeur Th and Le Guillou J C 1991 *Phys. Rev.* B **44** 2403
[21] Frésard R and Wölfle P 1992 *Proc. Conf. on Physics in Two Dimensions (Neuchâtel, 1991) Helv. Phys. Acta* at press
[22] John S, Voruganti P and Goff W 1991 *Phys. Rev.* B **43** 13365
[23] Dagotto E, Moreo A, Ortolani F, Poilblanc D, Riera F and Scalapino D 1991 *Static and Dynamical Properties of Doped Hubbard Clusters: Comparing Theory with Experiments* (Santa Barbara, CA: ITP, University of California)
[24] Frésard R, Dzierzawa M and Wölfle P 1991 *Europhys. Lett.* **15** 325
[25] Hirsch J E and Tang S 1989 *Phys. Rev. Lett.* **62** 591
Imada M and Hatsugai Y 1989 *J. Phys. Soc. Japan* **58** 3752
[26] Moreo A, Dagotto E, Jolicoeur Th and Riera F 1990 *Phys. Rev.* B **42** 6283
[27] Stephan W, von Szczepanski K J, Ziegler M and Horsch P 1990 *Europhys. Lett.* **11** 675
[28] Dagotto E, Moreo A, Joynt R, Bacci S and Gagliano E 1990 *Phys. Rev.* B **41** 9049
[29] Stephan W and Horsch P 1991 *Phys. Rev. Lett.* **66** 2258